

DESIGN AND ANALYSIS OF VTOL UAV

**Mr. Ronak Bharadwa*¹, Mr. Smit Daruwala*², Mr. Sonu Gajjar*³ Mr. Tejas Gajra*⁴,
Mr. Ankit Mandal*⁵, Prof. Asfakahemad Shekh*⁶**

*^{1,2,3,4,5}GTU, Mechanical Engineering Dept, Govt. Engineering College, Bharuch, Gujarat, India.

*⁶Assistant Professor, Mechanical Engineering Dept, Govt. Engineering College, Bharuch, Gujarat, India.

ABSTRACT

This project is based on VTOL UAV technology. UAV is important surveillance vehicle mainly used for armed forces operations but also it has capabilities making it helpful for common citizens. This project includes new aerodynamical designing of vehicle's various components like wing, fuselage, driving system, take-off landing advancements, simplicity to use, operating range, and analysis of components influenced by wind disturbance, altitude, power requirements. To optimize angle of attack of wings and tilt angle of propeller, so that maximum torque can be utilized for lift generation and minimize wind disturbances loss. Calculations include thrust force required to achieve necessary lift force, minimizing power loss due to drag and weight, type of driving system required, maximum flight time for given charge. Software used for designing are CAD (Solid works) and for analysis are CAE (Ansys). Project is mainly determined for reducing runway length, make UAV's Take-off and Landing easy as well as any terrain, and optimizing torque utilization.

Keywords: VTOL, UAV, Ansys, Solidworks, Airfoil, Flow analysis.

I. INTRODUCTION

The first ever recorded trial of an unmanned aerial vehicle for war occurred on July 1849, serving as a balloon carrier in the first offensive use of air power in aviation. Austrian forces besieging Venice launched 200 incendiary balloons at the besieged city. Maximum balloons were launched from land; however, few were also sent from the Austrian ship SMS Volcano. At least one bomb fell in the city; however, due to the wind disturbance, so most of them missed their aim, and few drifted back over Austrian lines and the launching ship Volcano [1].

The earliest attempt at a powered UAV was an "Aerial Target" in 1916. Tesla described a cluster of unmanned aerial vehicles in 1915. Advances followed during and after World War I, including the British Automatic Airplane in 1917 and the Larynx in 1927. These developments also inspired the construction of the Kettering Bug. Initially meant as an unmanned plane that would carry a payload to destroy desired target. The first remotely piloted vehicle was developed by film star and Reginald in 1935. More emerged during World War II with purpose to train anti-aircraft gunners and during fly attack missions. Nazi Germans produced and used various UAV aircraft during the war, like the Argus and the V-1 flying bomb driven by Jet engine. After World War II research & development continued in vehicles which resulted in vehicles like American JB-4, the Australian Teledyne Ryan Firebee I of 1951 and GAF Jindivik, while companies like Beechcraft introduced their models for the U.S. Navy in 1955 [1].

In 1959, the U.S.A.F, perturbed about losing pilots over hostile territory, started planning for utilising uncrewed aircraft. Planning got boost after the Soviet Union destroyed U-2 in 1960. Within days after which a highly classified UAV program commenced by the code name of "Red Wagon". The August 1964 in clash with North Vietnamese Navy America deployed highly classified UAVs (Ryan Model 147, Ryan AQM-91 Firefly, Lockheed D-21) Vietnam War was world's first war where America executed combat missions where UAV were used [1].

During the Attrition war (1967-1970) the first tactical UAV was first tested by the Israeli intelligence which was installed with cameras which helped in bringing photos across the Suez Canal. It was the first time that tactical UAVs that can take off and land on short runway (unlike the heavier jet-based UAVs) were developed and performed well in battle [1].

By 2013 at least 50 countries used UAVs. This includes US, Russia, China, Turkey, India, Iran, Israel and others designed and built their own varieties of UAV [1].

UAV is an aerial vehicle having no human on board presence while flying i.e., it is remotely operated by UAS intervention and with no pilot/human presence on board while in air. This research paper aims to provide system which can be used by anyone on the run for surveillance and mapping purpose, to expel runway

necessity for takeoff or landing of aerial vehicle, to give less maintenance, user friendly system, to make prototype to help Armed forces, farmers, security forces, delivery enterprises, mapping authorities, vigilance and ATS. Our main objective is to create CAD model of aerial vehicle, to create aerodynamically efficient vehicle system, to use brushless motor to provide quieter operation and modifying CAD model based on Analysis of model made on Ansys.

II. LITERATURE REVIEW

Table 1. Research papers referred

| Author | Title | Interest of study | Year |
|-------------------------------|---|---|----------|
| Vasile Prisacariu | CFD Analysis of UAV Flying Wing | Variation of lift vs drag at different Angle of attack and velocity | 2016 [2] |
| Sakhr Abudarag, Rashid Yagoub | Computational analysis of unmanned aerial vehicle | Computational validation of the UAV | 2017 [3] |
| Khuntia SK and Ahuja AS | Optimal Design and CFD Analysis of Wing of a Small-Scale UAV to Obtain Maximum Efficiency | Application of computational methods and iterative design process is explored | 2018 [4] |
| Ertugrul CETINSOY1 | Design and development of a tilt-wing UAV | Mechanism to control flight mode from hover to cruise and vice versa | 2010 [5] |
| Paul J. DeLorean | Vertical take-off and landing aircraft | Tilt mechanism was housed within fuselage at front and rear end | 2012 [6] |

III. METHODOLOGY

3.1 Mathematical Formulation

For the UAV analysis, the flow was assumed to be incompressible due to the maximum speed of 26.10 m/s. Therefore, only Navier-Stokes equations with the K-epsilon turbulence model and continuity equation were solved simultaneously [7].

3.2 Problem specifications

Chord length of airfoil: 1m

Free stream velocity: 51.45 m/s

Density: $1.1767 \frac{kg}{m^3}$

Co-efficient of viscosity: $1.009 \cdot 10^{-5} \frac{Ns}{m^2}$

3.3 Conversion of physical problem to mathematical model governing equations

$$\frac{\partial \bar{u}}{\partial x} + \frac{\partial \bar{v}}{\partial y} = 0 \tag{7}$$

$$\rho \left(\bar{u} \frac{\partial \bar{u}}{\partial x} + \bar{v} \frac{\partial \bar{v}}{\partial y} \right) = -\frac{\partial \bar{P}}{\partial x} + \mu \nabla^2 \bar{u} + \bar{f} turb_x \tag{7}$$

$$\rho \left(\bar{u} \frac{\partial \bar{u}}{\partial x} + \bar{v} \frac{\partial \bar{v}}{\partial y} \right) = -\frac{\partial \bar{P}}{\partial y} + \mu \nabla^2 \bar{v} + \bar{f} turb_y \tag{7}$$

$$\frac{\mu_t}{\rho} \approx \frac{C_\mu k^2}{\epsilon} \tag{7}$$

Conservation equation for k

Conservation equation for ϵ

The method which used for analysis is Finite Volume method and k-epsilon turbulence model.

3.4 K-epsilon turbulence model

K-epsilon (k- ϵ) turbulence model is model that is most widely used in Computational Fluid Dynamics (CFD) to imitate mean flow features and properties for turbulent flow conditions [8].

3.4.1 How it is analysed?

Using **K-epsilon (k- ϵ) equations**

This is two equation model that gives a general explanation of turbulence by means of two transport equations .

- The first transported variable is turbulent kinetic energy, k . It helps in determining the energy in the turbulence.
- The second transported variable is the turbulent dissipation, ϵ . It is the variable that helps in determining the scale of the turbulence.

3.4.2 Mathematically

The exact k- ϵ equation contain many unknowns and innumerable terms. For a much more practical approach, the standard k- ϵ turbulence model (Launder and Spalding, 1974) is used which is best suited for understanding relevant processes, thus decreasing unknowns and presenting a set of equations which can be applied to a large number of turbulent applications.

For turbulent kinetic energy k

$$\frac{\partial(\rho k)}{\partial t} + \frac{\partial(\rho k u_i)}{\partial x_i} = \frac{\partial}{\partial x_j} \left[\frac{\mu_t}{\sigma_k} \frac{\partial k}{\partial x_j} \right] + 2\mu_t E_{ij} E_{ij} - \rho \epsilon \quad [8]$$

For dissipation

$$\frac{\partial(\rho \epsilon)}{\partial t} + \frac{\partial(\rho \epsilon u_i)}{\partial x_i} = \frac{\partial}{\partial x_j} \left[\frac{\mu_t}{\sigma_\epsilon} \frac{\partial \epsilon}{\partial x_j} \right] + C_{1\epsilon} \frac{\epsilon}{k} 2\mu_t E_j E_{\dot{y}} - C_{2\epsilon} \rho \frac{\epsilon^2}{k} \quad [8]$$

here,

u_i represents velocity component in corresponding direction

E_{ij} components of rate of deformation

μ_t Represents eddy viscosity

$$\mu_t = \rho C_\mu \frac{k^2}{\epsilon}$$

IV. COMPUTATIONAL EXERCISE

4.1 UAV specifications:

Table 2. Specification

| | |
|---|--|
| b (Span) | 1.3 m |
| c (Chord Length) | 0.15 m |
| v_∞ (Velocity) | 20.0 m/s |
| ρ | 1.007 $\frac{kg}{m^3}$ |
| T | 20°C |

| | |
|-------------|---|
| μ_{air} | $1 \cdot 726 \times 10^{-5} \frac{Ns}{m^2}$ |
| g | $9.801 \frac{m}{s^2}$ |
| S | $0.195 m^2$ |
| W | $2.5 kg$ |

4.2 CALCULATION

Flight altitude to be 2000m above sea level

➤ Specification of wing

- $b = 1.3 m, L = 0.15 m, v_{\infty} = 20 m/s$
- Density of air = $1.007 \frac{kg}{m^3}$
- $T = 2^{\circ}C, \mu_{air} = 1 \cdot 726 \times 10^{-5} \frac{Ns}{m^2}, g = 9.801 \frac{m}{s^2}$

$$AR = \frac{b}{c}$$

$$AR = \frac{1.3}{0.15}$$

AR = 9

➤ Hence this is medium velocity UAV as it has AR=9 which is in the range of $8 < AR < 15$ for medium velocity UAV

$$Re = \frac{\rho v L}{\mu} = \frac{1.007 \times 20 \times 0.15}{1.726 \times 10^{-5}} \tag{7}$$

Re = 175028

Hence airfoil is selected from airfoil data base having following configuration

➤ Reynolds no. **2,00,000** for $N_{CRIT} = 9, (C_L/C_D)_{max} = 38.91$ at $\alpha = 2.5,$ [9]

As it's known that for the cruise flight $Weight(W) = Lift(L)$

$$W = L$$

$$W = \frac{1}{2} \rho v_{\infty}^2 (s) (C_L) \tag{10}$$

$$C_L = \frac{2.5 \cdot 9.801 \cdot 2}{20 \cdot 20 \cdot 1.007 \cdot 0.195}$$

$C_L = 0.6239$

Selecting $C_L = 0.6312$ from tools at $\alpha = 6$ as this is nearest value with respect to calculated value and for same Angle of attack, we will select Co-efficient of drag,

$C_D = 0.03926$

$$L = \frac{1}{2} \rho v_{\infty}^2 (s) (C_L) \tag{10}$$

$$= \frac{1.007 \cdot 20^2 \cdot 0.195 \cdot 0.6239}{2}$$

L = 24.78 N

$$D = \frac{1}{2} \rho v_{\infty}^2 (s) (C_D) \tag{10}$$

$$= \frac{1.007 \cdot 20^2 \cdot 0.195 \cdot 0.03926}{2}$$

D = 1.54186 N

Table 3. L & D variation with α

| Sr. No. | Angle of Attack (in Deg.) | Lift (in N) | Drag (in N) |
|---------|---------------------------|-------------|-------------|
| 1. | 2 | 10.09 | 0.29 |
| 2. | 4 | 17.22 | 0.55 |
| 3. | 6 | 24.78 | 1.54 |
| 4. | 8 | 27.78 | 2.99 |

For the calculation of T_{Rmin} ,

$$K = \frac{1}{\pi e AR} \quad \text{take } e = 0.85 \quad [10]$$

$$K = \frac{1}{\pi * 0.85 * 9}$$

K = 0.0416

From the air-foil database, we can select Co-efficient of Lift and Co-efficient of Drag at maximum Lift to drag ratio as given below

$$C_{L(l/d) \max} = 0.3058, C_{D(l/d) \max} = 0.00786$$

$$C_{D0} = C_{D(l/d) \max} - K(C_{L(l/d) \max})^2$$

C_{D0} = 0.00378

$$T_{Rmin} = W\sqrt{4KC_{D0}} \quad [10]$$

$$T_{Rmin} = 2.5 * \sqrt{4} * \sqrt{0.0416} * \sqrt{0.00378}$$

T_{Rmin} = 0.062 N

For achieving T_{Rmin} Pilot needs to throttle velocity up-to V_{Rmin}

$$V_{Rmin} = \frac{\sqrt{2}(\frac{W}{S})}{\rho} * \sqrt[4]{(\frac{K}{C_{D0}})} \quad [10]$$

V_{Rmin} = 9.18 m/s

V. PREPARING 3D MODEL

Initially for practising purpose model of already in service UAV was made and it is as shown in figures after this model it was clear solidworks is gives satisfactory results so moving ahead model was prepared based on our calculations to give it optimum aerodynamic help and good aesthetic appearance [11].

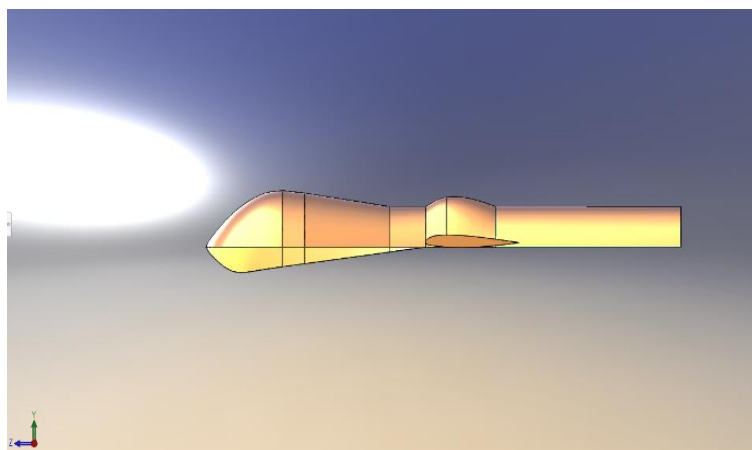


Fig 1: Practice Model (Side View)

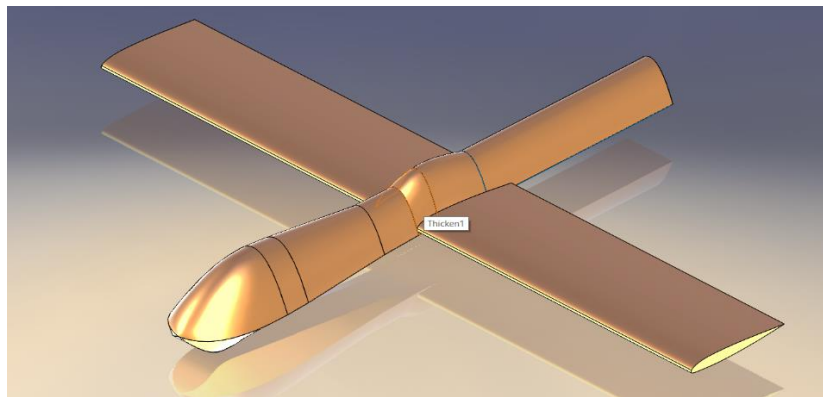


Fig 2: Practice Model (Isometric View)

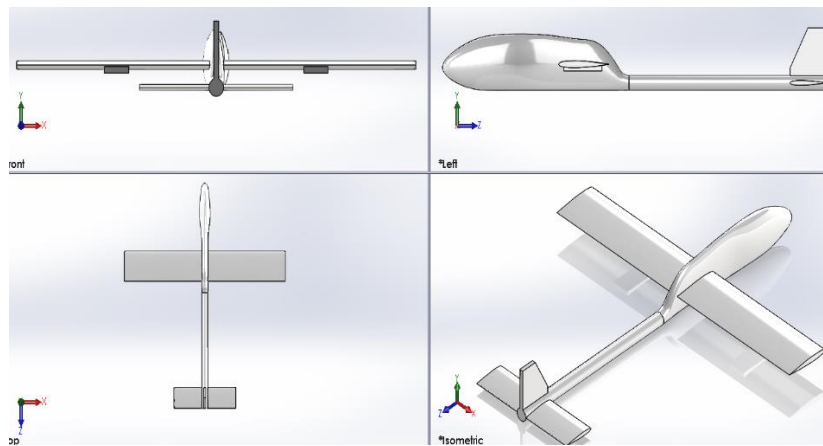


Fig 3: Model Views

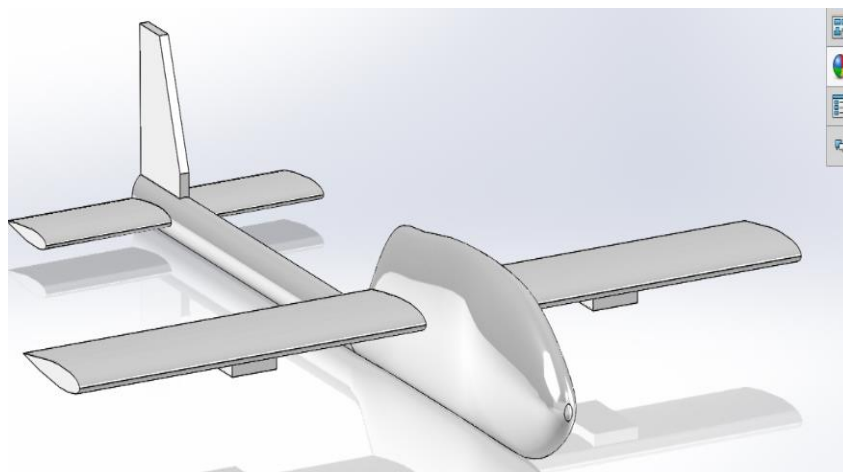


Fig 4: Isometric view of model

5.1 VTOL Mechanism on Solidworks

For VTOL commencement of UAV, it was necessary to provide guide to propellers to that they can tilt 90 for generating lift for taking off figure below shows VTOL mechanism which will have housing for battery, propeller, shaft, and tilting mechanism by help to which VTOL will be held [10].

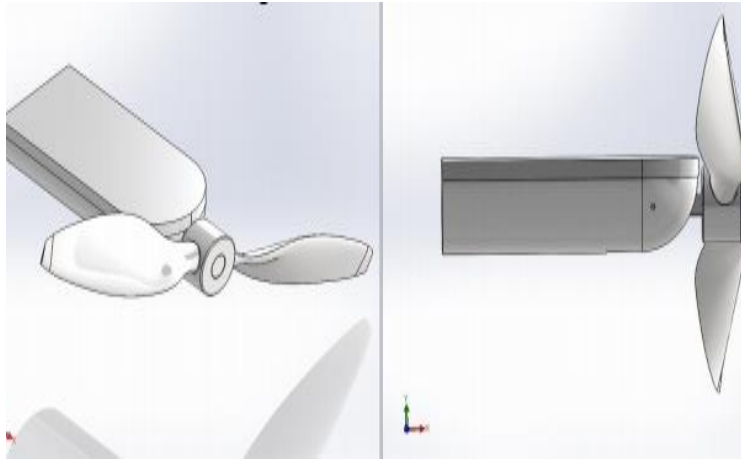


Fig 5: VTOL Mechanism



Fig 6: Brushless motor



Fig 7: Propeller

Above figure show brushless motor and propeller to be selected for UAV specification of battery is A60- 18M, 35V, 46.2 Amp, 6136 RPM, 1618W power and propeller name is APC thin electric 20 * 11

VI. GEOMETRY AND MESH

Meshing is an integral part of the computer-aided engineering (CAE) simulation process. The mesh influences the accuracy, convergence and speed of the solution.

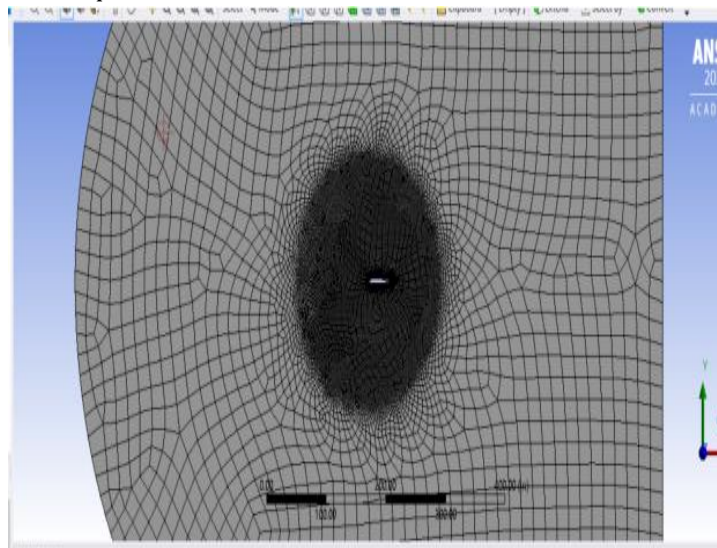


Fig 8: Mesh

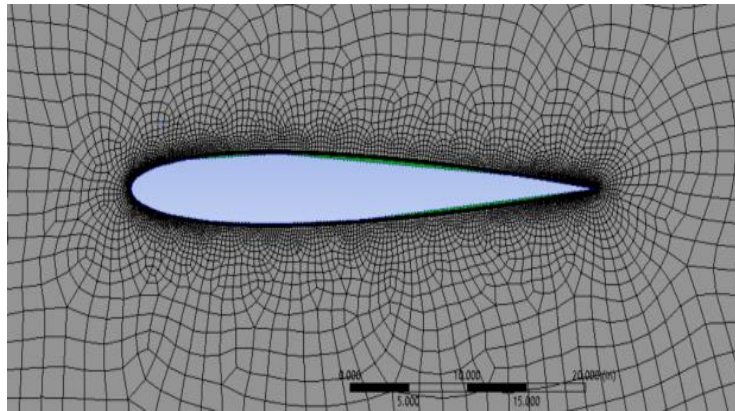


Fig 9: Mesh

6.1 Mesh Size

Number of mesh element are 27526. Unstructured grid with triangles and tetrahedral in the surface and volume meshes was implemented.

6.2 Boundary layer Consideration

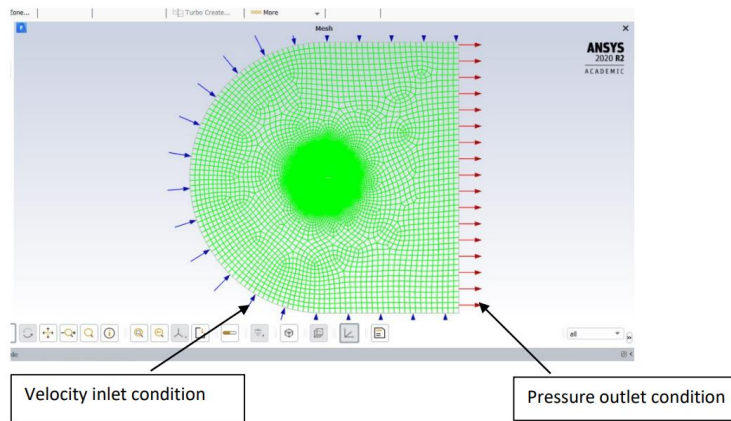


Fig 10: Boundary Conditions

Boundary conditions were applied, on the left boundary of the flow domain which was named far field 1 a velocity inlet condition was applied. The magnitude of X-component of velocity is 50.22 m/s and Y-component is 8.85m/s. A pressure outlet condition was applied on the right end of the flow domain (farfield2) which was equal to atmospheric pressure Initialization of the problem was done based on the far field 1 conditions Report parameters like lift coefficient, drag coefficient were introduced. The numerical method initially used was first order, the solution seemed stable but values were not close to the experimental values, then second order cell center method was used over 1000 iterations. Convergence criteria applied was absolute

VII. RESULTS AND DISCUSSION

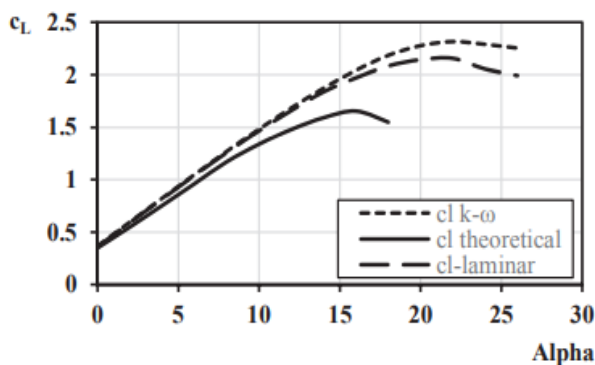


Fig 11: Lift coefficient vs angle of attack (α)

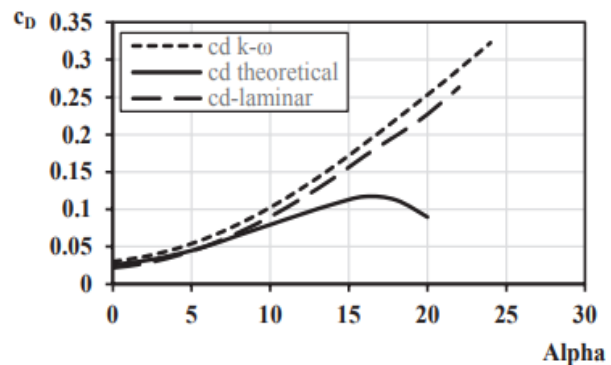


Fig 12: Drag coefficient vs α

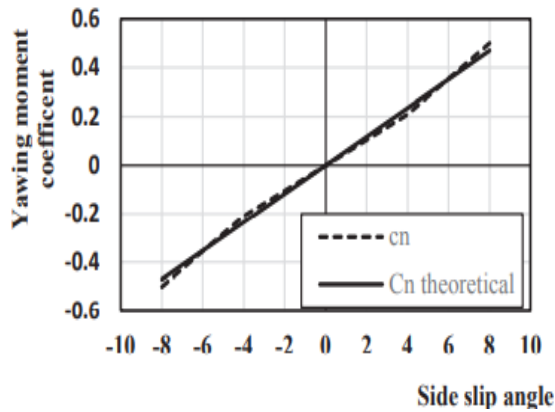


Fig 13: Yawing moment coefficient vs slip side angle

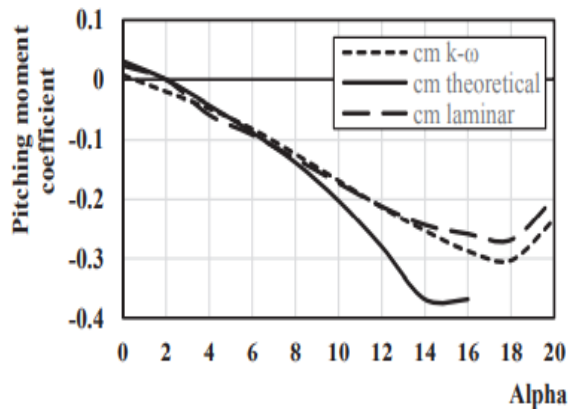


Fig 14: Pitching moment coefficient vs angle of attack

Figure 11 shows the variation of the lift coefficient versus angle of attack at $R_E = 1.126 \cdot 10^6$ for the designed UAV according to the type of model used. The maximum lift coefficient for the theoretical calculation is 1.7 occurs at angle of attack 16 degrees, whereas for both computational models is occurred approximately at angle of attack 22 degrees, but with different maximum lift coefficient. The maximum lift coefficient for turbulent model is 2.3, whereas for the laminar model is 2.2. It is observed that the results obtained from the computational analysis of UAV for the two models was agreeable at a low angle of attack ($0 < \alpha < 10$) but by increasing angle of attack there is a significant difference in maximum lift coefficient value. The difference or the delay in stall angle for computational analysis might reveal to steady state assumption. Figure 12 represents the curve of drag coefficient versus angle of attack. The graphical curve for drag coefficient is almost indicating the similar trend. Therefore, the good agreement between the two methods used for determining the drag coefficient is definitely able to validate the accuracy of the analysis work in the present study [3]. Figure 13 shows the correlation between yawing moment coefficient and side slip angle (β). The airplane is said to be directionally stable if it has an inherent capability to realign itself into the resultant wind whenever disturbed from steady level flight. Mathematically, the requirement for directional stability criterion is that $C_{N\beta} > 0$, and from this figure, it is obvious that this criterion is satisfied. The variation of moment coefficient versus angle of attack is indicated by Figure 14. The moment coefficient values start positive and then decrease gradually until the trim point where they become negative. The positive moment coefficient at zero angle of attack (C_{M0}) and the negative moment coefficient variation with angle of attack are satisfied the requirement of longitudinal stability criterion. The value of negative ($C_{M\alpha}$) and positive ($C_{N\beta}$) demonstrate that the UAV is statically stable [3].

7.1 Computational results:

7.1.1 Scaled residuals

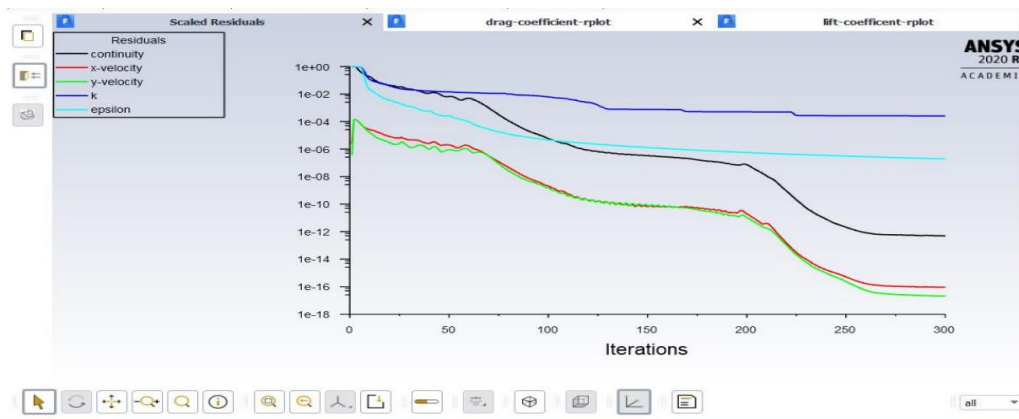


Figure 15: Scaled Residuals after 300 iterations using second order method

7.1.2 Drag coefficient

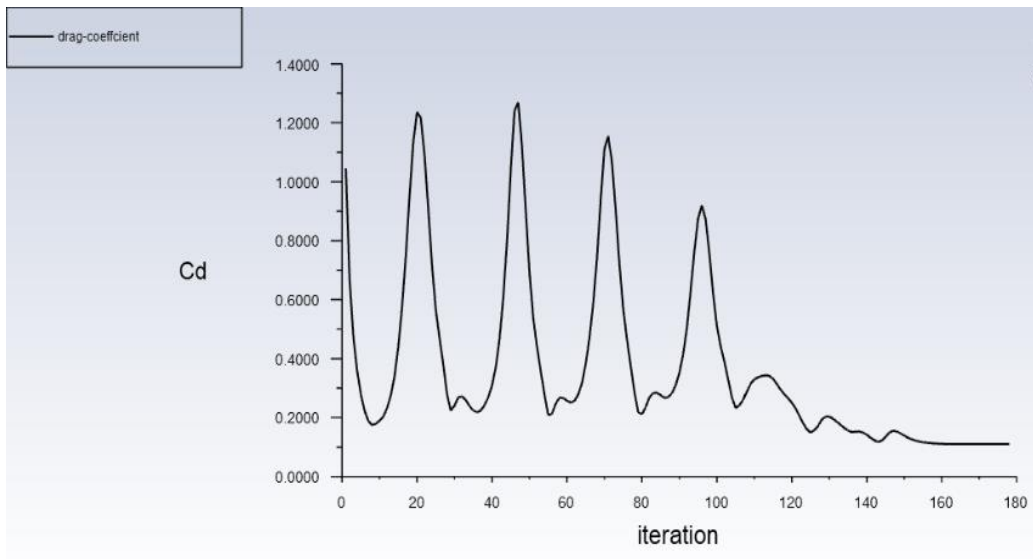


Figure 16: Drag coefficient after 300 iterations which converged to value 0.052

7.1.3 Lift coefficient

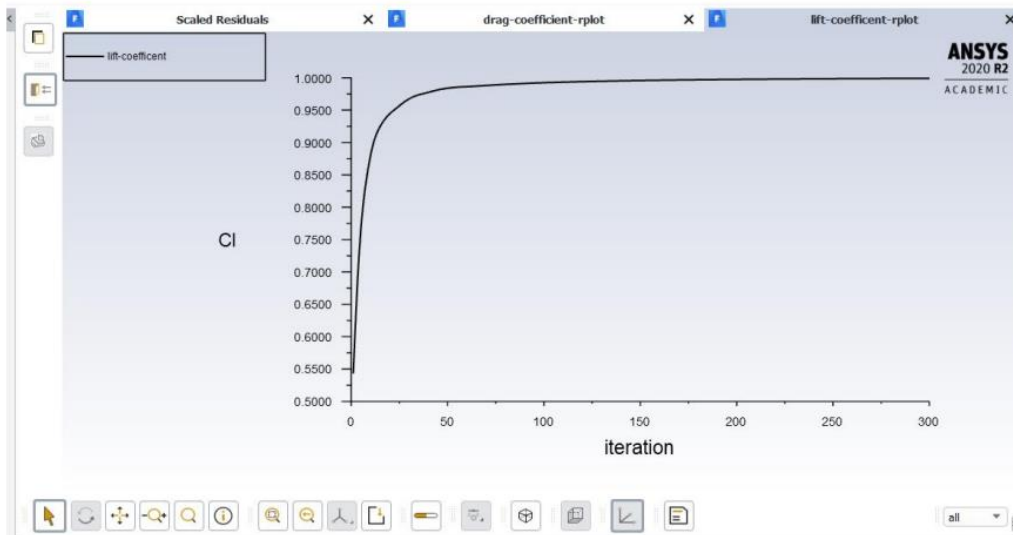


Figure 17: Lift coefficient after 300 iterations which converged to value 1.02

7.1.4 Pressure Contour

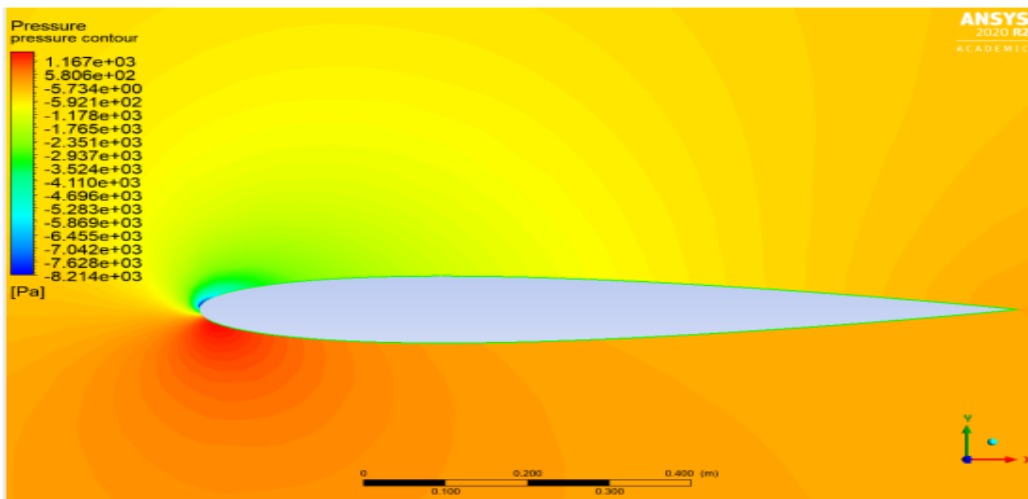


Figure 18: Pressure contour

A line connecting points of equal height of a given barometric pressure; the intersection of a constant pressure surface by a plane parallel to mean sea level. Figure 18 represents the pressure contour at MAC for the horizontal tail before the stall at angle of attack 10 degrees. The horizontal tail is symmetric air-foil, but according to angle of attack the distribution of pressure is cleared. Constant pressure is captured from the leading edge to about 25% of the wing chord. Then the effect of the Dirichlet boundary condition is verified. The pressure on the pressure side is greater than the pressure on the suction side. The pressure distribution on the upper surface of the tail is predicted [3].

7.1.5 Pressure Coefficient

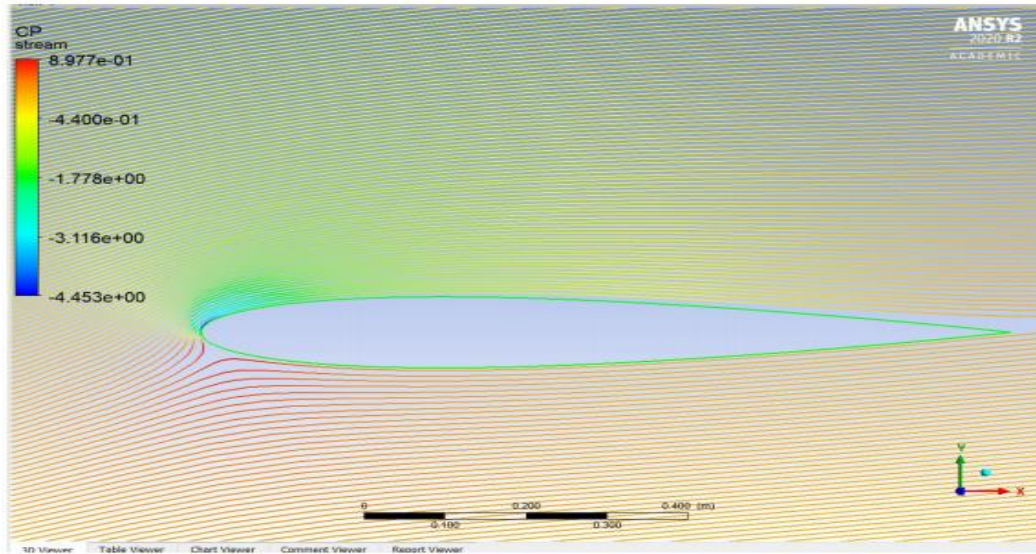


Figure 19: Pressure coefficient

The pressure coefficient is a dimensionless number which describes the relative pressures throughout a flow field in fluid dynamics. It is used in hydrodynamics and aerodynamics. Every point in a fluid flow field has its own unique pressure coefficient, C_p [12].

In the figure 19, it can be observed that pressure coefficient is high at the lower end of leading edge and low at the upper end, which leads to generation of lift. Pressure coefficient result was used to study the incompressible air flow over the airfoil. To test the design, pressure coefficient was calculated at critical locations around the airfoil and these values were used to predict values along the whole model. It was also observed that the pressure coefficient values increase as the angle of attack increases. The pressure coefficient values obtained from simulation were compared with experimental results. Pressure coefficient is dimensionless quantity which is defined as the ratio of local pressure to the stagnation (dynamic) pressure, mathematically it is stated as follows

$$C_p = \frac{p - p_\infty}{\frac{1}{2} \rho_\infty v_\infty^2} = \frac{p - p_\infty}{p_0 - p_\infty} \quad [12]$$

where:

p is the static pressure at the point at which pressure coefficient is being evaluated?

p_∞ is the static pressure in the freestream (i.e. remote from any disturbance)

p_0 is the stagnation pressure in the freestream (i.e. remote from any disturbance)

ρ_∞ is the freestream fluid density (Air at sea level and 15 °C is 1.225 kg/m³)

V_∞ is the freestream velocity of the fluid, or the velocity of the body through the fluid

7.1.6 Velocity contour

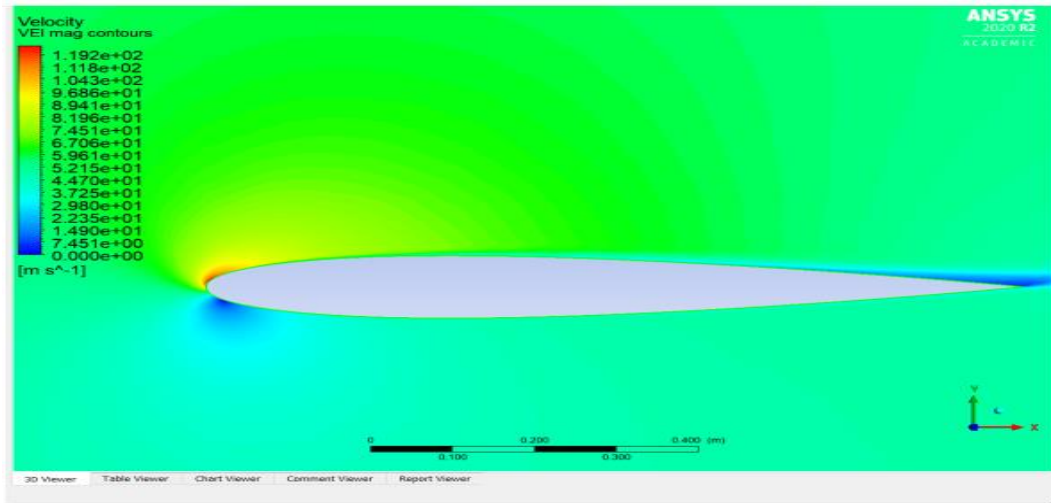


Figure 20: Velocity contour

7.1.7 Velocity vectors

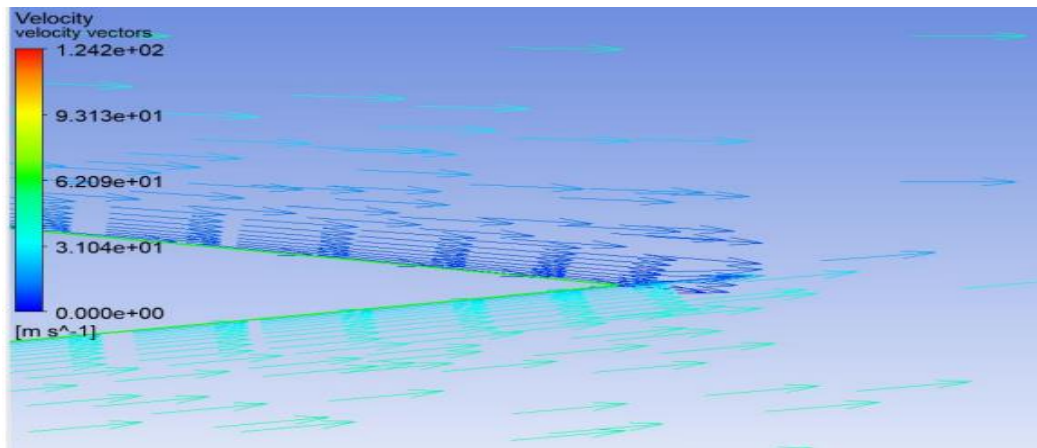


Figure 21: Velocity contour near the trailing edge. No flow separation is observed

Determination of the discharge of a stream by measuring the elemental areas between successive isohels and summing the products of each area by the mean of its boundary velocities. Figure 20 illustrates the flow path lines over the upper surface of wing before the stall at angle of attack 10 degrees. It is obvious there are no vortex existence and the flow moves linearly. Figure 21 shows the flow path lines after the stall at angle of attack equal to 10 degree. In this figure, the existence of vortex on upper surface and tip vortices are indicated [3].

7.1.8 Turbulent Kinetic Energy Contour

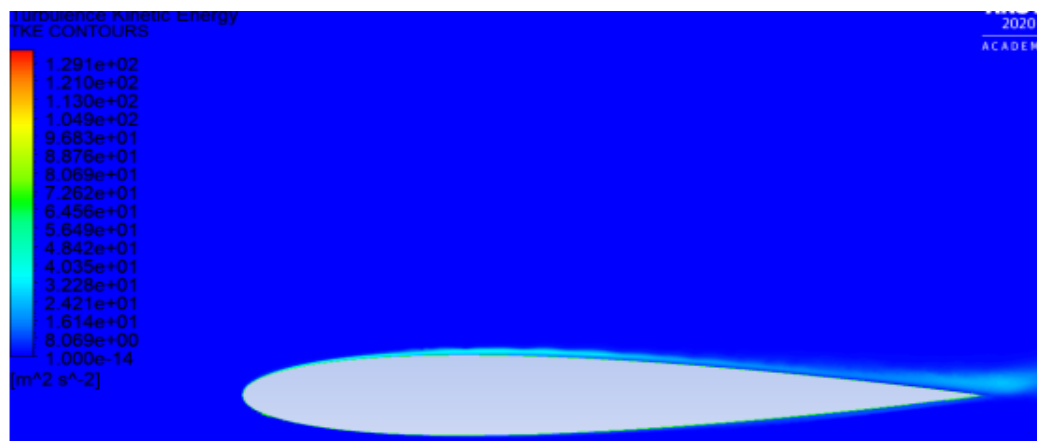


Figure 22: Due to steep velocity gradient near the boundary of air foil slight turbulence is present

Turbulence kinetic energy (TKE) is the mean kinetic energy per unit mass associated with eddies in turbulent flow. In the Reynolds-averaged Navier Stokes equations, the turbulence kinetic energy can be calculated based on a turbulence model.

An equation for the fluctuating kinetic energy for constant density flow can be obtained directly from the Reynolds stress equation derivation (by contracting the free indices) [13].

The result is:

$$\left[\frac{\partial}{\partial t} \langle u_i u_i \rangle + U_j \frac{\partial}{\partial x_j} \langle u_i u_i \rangle \right] = \frac{\partial}{\partial x_j} \left\{ -\frac{2}{\rho} \langle p u_i \rangle \delta_{ij} - \langle q^2 u_j \rangle + 4\nu \langle s_{ij} u_i \rangle \right\} - 2 \langle u_i u_j \rangle \frac{\partial U_i}{\partial x_j} - 4\nu \left\langle s_{ij} \frac{\partial u_i}{\partial x_j} \right\} \quad [12]$$

VIII. VERIFICATION AND VALIDATION

1. Sanity check was performed from the results. No discrepant result was observed
2. Boundary conditions satisfied the mathematical model

For validation, experimental results available on the NASA's website were compared

https://turbmodels.larc.nasa.gov/naca0012_val.html

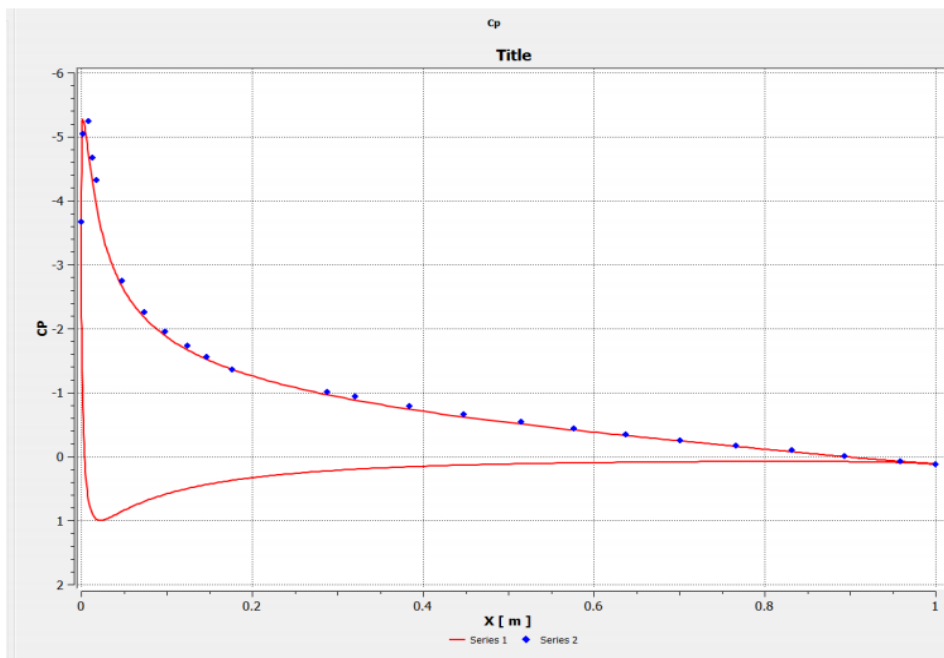


Figure 23: Graph of Cp (Pressure coefficient over the air-foil)

Series 1: Pressure coefficient obtained from my results over the air-foil

Series 2: Graph Imported from NASA's experimental result for the upper part of air-foil

A sweet overlap is observed so it can be concluded that the results obtained are correct

IX. CONCLUSION

A conforming overlap is observed between series 1 and series 2 graph so it can be concluded that the results obtained are correct. No flow separation was present as it can be observed from the velocity vectors plot. The aircraft will have a steady flight for the given conditions. The values of lift coefficient and drag Coefficient were really close to experimental values obtained from Ladson force data from NASA [14].

X. REFERENCES

- [1] https://en.wikipedia.org/wiki/Unmanned_aerial_vehicle#History.
- [2] https://www.researchgate.net/publication/307947707_CFD_Analysis_of_UAV_Flying_Wing.
- [3] <https://aip.scitation.org/doi/abs/10.1063/1.4972593>.
- [4] <https://www.longdom.org/abstract/optimal-design-and-cfd-analysis-of-wing-of-a-small-scale-uav-to-obtain-maximum-efficiency-17249.html>.

- [5] <https://journals.tubitak.gov.tr/elektrik/abstract.htm?id=11957>.
- [6] <https://www.wired.com/story/delorean-aerospace-flying-car/>.
- [7] J. Anderson, "Computational Fluid Mechanics and Heat Transfer," CRC.
- [8] "cfd-online.com," CFD online, [Online]. https://www.cfd-online.com/Wiki/K-epsilon_models.
- [9] Airfoil tools [Online]. <http://airfoiltools.com/>
- [10] A. J. Keane, Small unmanned fixed-wing aircraft design- A Practical approach, Wiley.
- [11] R. Austin, Unmanned Aircraft systems.
- [12] J. Anderson, Fundamental of Aerodynamics.
- [13] "CFDonline,"[Online].
- [14] Available:https://www.cfdonline.com/Wiki/Introduction_to_turbulence/Turbulence_kinetic_energy.
- [15] [Turbmodel.larc.nasa.gov](http://turbmodels.larc.nasa.gov)
https://turbmodels.larc.nasa.gov/NACA0012_validation/CLCD_Ladson_expdata.dat